

# **Title:** Bioinspired Soft Spiral Robots for Versatile Grasping and Manipulation

## **Authors:**

Zhanchi Wang<sup>1</sup>, Nikolaos M. Freris<sup>1\*</sup>

## **Affiliations:**

<sup>1</sup> School of Computer Science and Technology, University of Science and Technology of China, Anhui, China.

\*Corresponding author. Email: nfr@ustc.edu.cn.

**Abstract:** Across various species and different scales, certain organisms use their appendages to grasp objects not through clamping but through wrapping. This pattern of movement is found in octopus tentacles, elephant trunks, and chameleon prehensile tails, demonstrating a great versatility to grasp a wide range of objects of various sizes and weights as well as dynamically manipulate them in the 3D space. We observed that the structures of these appendages follow a common pattern - a logarithmic spiral - which is especially challenging for existing robot designs to reproduce. This paper reports the design, fabrication, and operation of a class of cable-driven soft robots that morphologically replicate spiral-shaped wrapping. This amounts to substantially curling in length while actively controlling the curling direction as enabled by two principles: a) the parametric design based on the logarithmic spiral makes it possible to tightly pack to grasp objects that vary in size by more than two orders of magnitude and up to 260 times self-weight and b) asymmetric cable forces allow the swift control of the curling direction for conducting object manipulation. We demonstrate the ability to dynamically operate objects at a sub-second level by exploiting passive compliance. We believe that our study constitutes a step towards engineered systems that wrap to grasp and manipulate, and further sheds some insights into understanding the efficacy of biological spiral-shaped appendages.

**One-Sentence Summary:** Design, fabrication, and operation of spiral soft robots at variable scales that can manipulate objects through wrapping.

## **Main Text:**

### **INTRODUCTION**

Wrapping as a paradigm for grasping and manipulation (1), which are two key objectives in robotics (2, 3), is found in the prehensile tail of chameleons and seahorses with length scales as small as a few millimeters (4), as well as in the tentacles of octopuses and the trunks of elephants as large as a meter (Fig. 1A) (5, 6). These structures curl from their tips, tightly wrap around objects of different sizes and shapes, and continuously control the curling direction to manipulate them with unmatched efficiency (Fig. 1B). Roboticians have successfully achieved effective control of an object's motion using grasping - defined as the force-closure of an object (7). For example, clamping (8), digging (9), hooking (10), vacuum suction (11), magnetic attraction (12), and so on. Nevertheless, grasping and manipulating objects through wrapping remains by-and-large unaddressed, noting the succinct difference between the continuous deformation/compliant interaction (13) exhibited by biological systems and the discrete joints/rigid materials employed in robotic systems (7) that scientists and engineers have long worked on.

Soft robots (13–17) made of flexible materials are well tailored to produce continuous deformations and interact with the environment (18–20). In particular, soft manipulators have shown high compliance and adaptability, enabling the development of grippers capable of grasping in an

---

enveloping (21–23) or twisting (24–27) manner. Although there is a growing interest in developing systems that can grasp/manipulate objects through wrapping (28–33), existing soft robots fail to achieve biologically comparable versatility. Taking an elephant as an example, its trunk can wrap a carrot with a diameter of 3 cm, while it can also grasp and stack 300 kg stumps over half a meter in diameter. We argue that this gap can be filled by morphologically replicating the spiral patterns that are ubiquitous in nature.

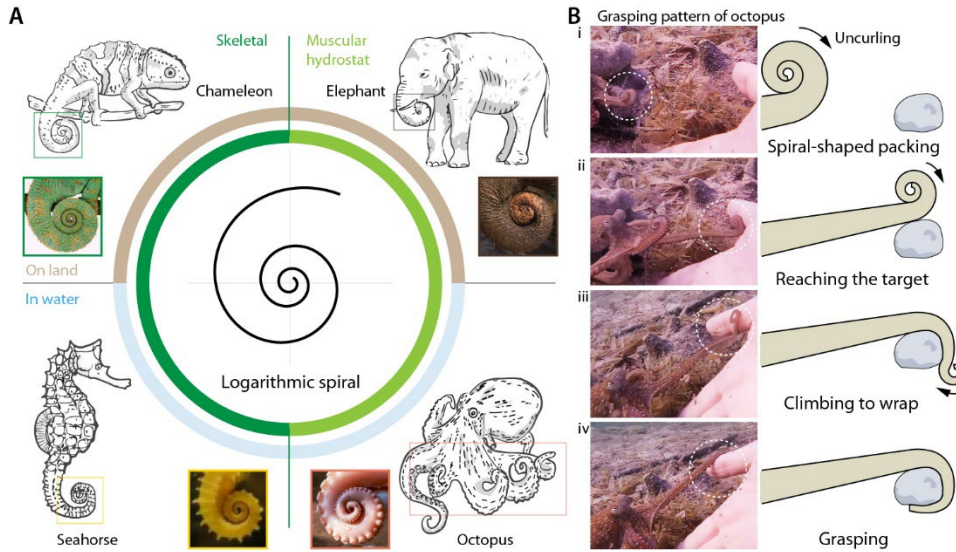


**Fig. 1. Overview of the motivation and inspiration of the soft spiral robot.** (A) Examples of animal parts that follow the logarithmic spiral pattern, which is found primarily used for grasping and manipulating organs. (B) The octopus moves its tentacle to grasp an object in four stages: i) extending toward the object, ii) making contact, iii) climbing to wrap, and iv) grasping (original video credits: <https://www.youtube.com/watch?v=GdCOYToDqfM>).

We describe two principles that help enable a basic recreation of the spiral-shaped curling behavior in an artificial system. First, we present a logarithmic-spiral-based design that allows the curling to be achieved with single cable actuation; this can be further extended to designing multi-cable spiral robots that are capable of more complex deformations in the 3D space. Second, we develop a bioinspired grasping strategy that adapts to a variety of objects without requiring prior knowledge about their shape. The combination of these two principles gives rise to a series of cable-driven soft spiral robots (SpiRobs) that can effectively grasp and dynamically manipulate objects of various sizes, shapes, and weights.

## RESULTS

### Design of SpiRobs

The first principle is based on the uncurling of a logarithmic spiral and is the key to enable a parametric design scheme that allows easy fabrication across scales. The uncurred spiral results in a tapered body, which can be curled and wrapped back into a spiral under the forces acting through a cable (Fig. 2A). This design concept is a goal-directed reverse engineering process that ensures a large continuous change in the curvature of the body which, in turn, constitutes the basis for grasping objects of different sizes. The cable passes through the body of the robot with one end fixed to the tip through a knot and the other connected to the motor (Fig. 2B). A thin elastic layer serves to connect discrete units. This design allows to achieve basic curling and uncurling with just one cable; when the cable is relaxed, the elastic layer provides the restoring force for uncurling (Fig.

2B and movie S1). Notably, the passive compliance inherent in the elastic layer enables the robot to interact safely with the environment and further allows to generalize the design to multi-cable robots with simple control laws.

The **logarithmic spiral** (represented in polar coordinates  $(\rho, \theta)$  by  $\rho = ae^{b\theta}$ , where  $a$  and  $b$  are scaling parameters), also known as growth spiral, is found in nature across species and scales (Fig. 2C). SpiRobs are designed directly from the mathematical expression for the spiral via the following process. The rays starting from the origin that correspond to fixed angle intervals  $(\Delta\theta)$  intersect with points on the spiral that are connected to form quadrilateral areas: these are the design blocks for building the robot units (Fig. 2D). Note that once the spiral parameters and discretization step  $(\Delta\theta)$  are given, the dimensions of the robot units are fully determined; in fact, adjacent units are in a fixed ratio (see MATERIALS AND METHODS section 'Fabrication of SpiRob') which allows for a modular fabrication. The curvature of SpiRobs changes exponentially fast with  $\theta$  (it can be arbitrarily large/small when the value of  $\theta$  tends to  $-\infty/+\infty$ ) and this provides a justification for the ability to grasp at different scales. Regarding the effect of design and fabrication, note that most soft robots use homogeneous materials that are generally incompressible (such as silicone) to build continuous bodies and are thus prone to buckling (34). In contrast, the proposed SpiRobs feature (by design) uniform gaps among the discrete units which provide space for the body to deform; when the gaps are fully squeezed, the robot curls into a spiral shape. Based on the same principle, we can design and fabricate spiral-shaped robots capable of movements in the 3D space with multi-cable actuation (Figs. 2E, S1, and S2).

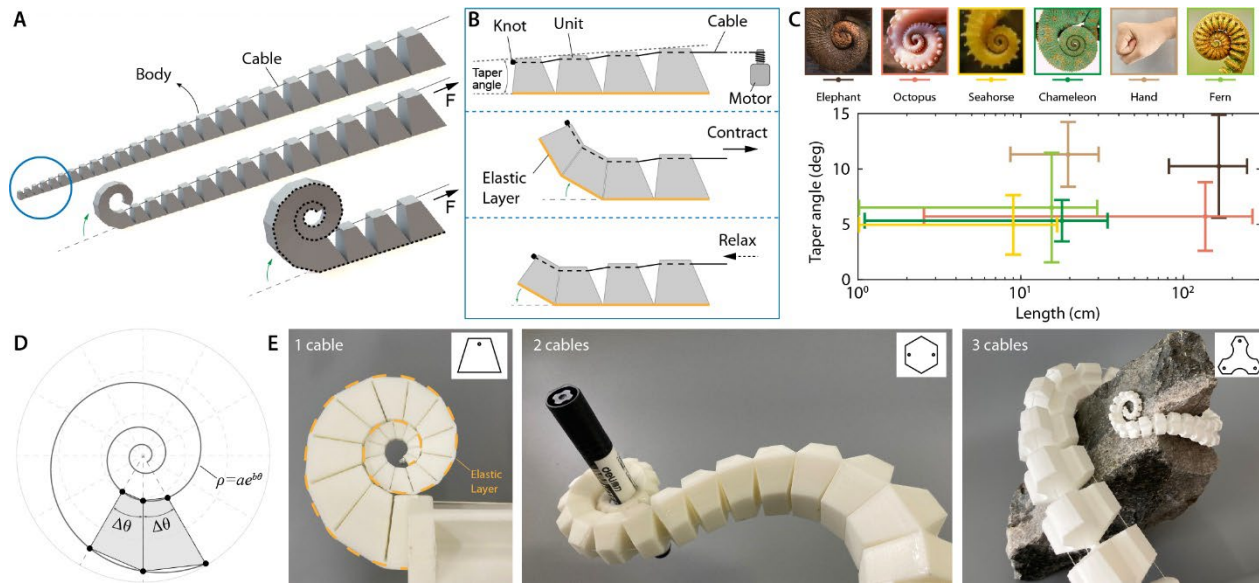


**Fig. 2. Design of bioinspired soft spiral robots.** (A) A computer-aided design (CAD) model of a 25 cm long SpiRob driven by a cable. The robot consists of a series of discrete units with a cable running through them. The top-to-bottom image sequence shows curling from the tip when the cable is stretched. The blue circled region of the robot's tip transmission is magnified in (B): Enlarged top view of the robot's motor-cable-body assembly. The body of the robot consists of a series of units, connected by an elastic layer. The contour (dashed lines in the first panel) forms a cone with a fixed taper angle. A motor is connected to the cable which is attached to the tipmost unit by a knot. The cable contraction and relaxation (second and third panels, respectively) are translated into the robot curling and uncurling motion. (C) Illustrations of the length scales and taper angles of spiral-shaped wrapping appendages in nature. The length information was obtained from Encyclopedia Britannica, and the taper angle information was measured based on pictures of different individuals. (D) Illustration of a SpiRob tightly packed into a logarithmic spiral ( $\rho = ae^{b\theta}$ );  $\Delta\theta$  is the discretization step. (E) Images of soft spiral robots driven by a single cable, two cables, and three cables, with corresponding cross sections shown in the upper right corner.

A salient feature of our proposed design lies in the choice of taper angle. This trait has also been observed in nature, for example different taper angles exist across various species of the octopus. We designed three spiral robots of variable taper angle ( $5^\circ$ ,  $10^\circ$ , and  $15^\circ$ ) with the same length and tip diameter (Fig. 3A). We found that the envelope of the workspace of a spiral robot also follows a spiral shape (Fig. S5 and Text S5). Moreover, simulations validate that all of the interior is reachable (Fig. 3B). The following conclusions are drawn for fixed length and tip diameter. The smaller the taper angle, the larger the workspace (Fig. 3B). At the same time, the larger the taper angle, the smaller the diameter of the smallest object that can be grasped and the larger the maximum load capacity; besides, for fixed diameter, the larger the weight (with the difference more pronounced for large-sized objects, see Fig. 3C and Text S5). Taking the robot with a taper angle of  $15^\circ$  as an example, it can grab objects whose diameters vary by two orders of magnitude (from 5.6 mm to 108 mm) and weigh roughly 260 times the weight of the robot (38.4 g self-weight and 10 Kg load capacity, see Fig. 3D, and Text S5 for theoretical justification).

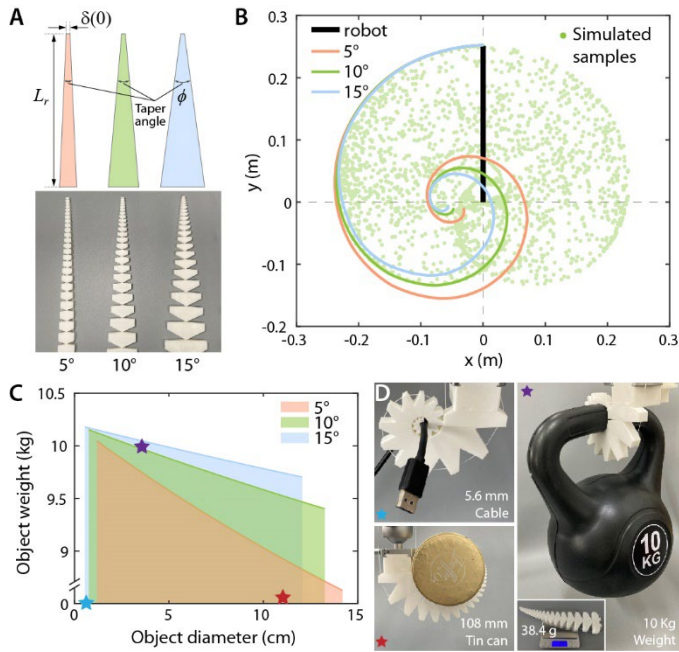


**Fig. 3. The effect of taper angle on the workspace and grasping ability.** (A) SpiRobs with different taper angles:  $5^\circ$ ,  $10^\circ$ , and  $15^\circ$ ;  $L_r$  is the length of the robot and  $\delta(0)$  is the width of its tip ( $L_r = 25$  cm and  $\delta(0) = 5.5$  mm in this case). (B) Workspace: the smaller the taper angle, the larger the workspace, which translates to more flexibility. The envelope of the workspace also follows a logarithmic spiral (plotted in different colors for each taper angle). The green dots illustrate the workspace for a taper angle of  $10^\circ$ , as generated by randomly sampling cable forces in simulation. (C) Theoretical predictions of the object size and weight that can be grasped with a maximum actuation force of 100 N: a larger taper means larger weight for fixed diameter. (D) Images of a SpiRob ( $15^\circ$  taper angle) grasping a 5.6 mm diameter cable, 108 mm diameter can, and 10 kg weight. Stars in (C) and (D) are used to match the experiments to the weight-diameter plot.

## Bioinspired grasping strategy

The second principle that we leverage enables the active control of the curling direction so as to wrap to grasp and manipulate different objects. A similar movement pattern is observed in octopus tentacles when interacting with the environment (Fig. 1B and movie S2). In our system, we implement this by controlling the cable forces. Take the robot actuated by two cables as an example (Fig. 4A): when only the left or right cable is stretched, it is capable of curling in the two directions and can be tightly packed into a spiral shape. By jointly controlling the forces exerted by the two cables, the robot reaches out, contacts the object, and uncurls the packed body along the object surface to wrap it (Fig. 4 B, C, S3, and movie S2). In quasi-static operations, the tip of the robot forms a stable structure under the action of antagonistic forces from the two cables. A distinctive attribute of the robot operation is that it always starts to curl/uncurl from the unit closest to the root when changing the force on one side (while keeping the other one fixed). To this end, the elastic layer on the central axis is instrumental to the uncurling of the packed body in order to reach out in different directions (Fig. S3, movie S2, and Text S2). Based on this working principle, it is possible to control the robot to grasp objects on a two-dimensional plane (Fig. 4C) by varying the actuation



forces through the two cables (Fig. 4D). We have verified the effectiveness of this grasping and manipulation principle on both real robots (Fig. 4E) and in simulations (where we use a model based on serial elastic joints, see Fig. S4 and text S4). Different from existing fingertip-based grasping paradigms (8), the proposed strategy utilizes all the surfaces of the robot to contact and wrap around the object. This is advantageous because a larger contact area means greater load capacity and grasping stability. Moreover, this strategy is distinguished from the "whole-arm-grasping" paradigm (35), since it is not only the contact between the robot surface and the object but also the contact and extrusion with itself that are leveraged for grasping and manipulation. We would like to highlight that when the packed body uncurled along the surface of the object, a behavior similar to the "climbing" of a plant vine that navigates without friction from sliding against the environment was generated: this enables the robot to adapt to objects of different geometries regardless of their surface roughness.

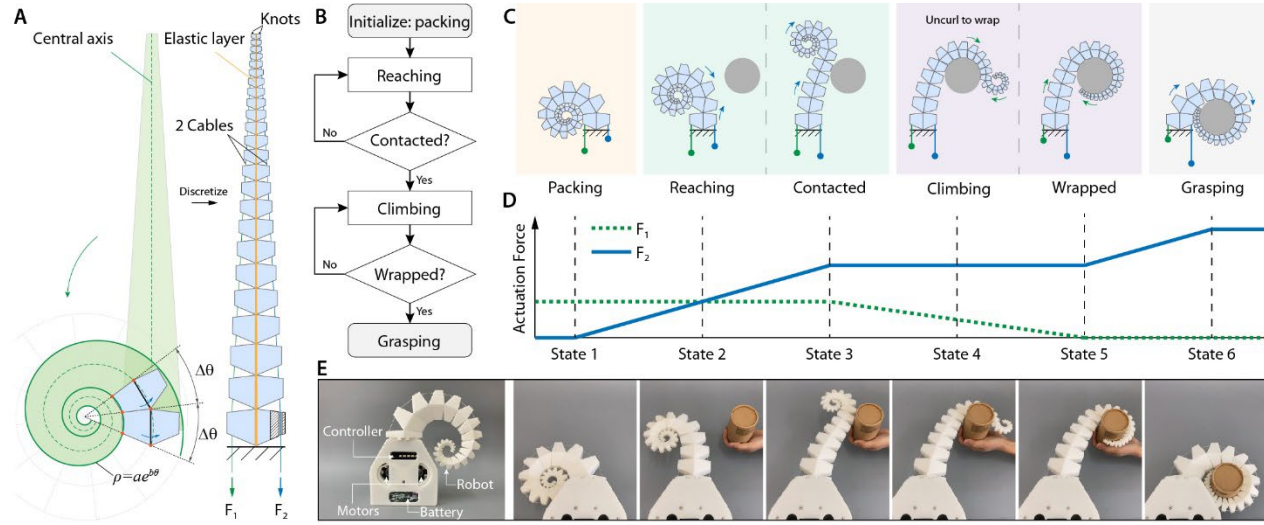


**Fig. 4. The principle of asymmetric cable forces enabling active curling, wrapping, and grasping.** (A) Illustrations of the design of a SpiRob driven by two cables passing through the body and fixed to the tip with two knots. The central axis of the robot comprises an elastic layer. The design parameters of the robot can be determined by a logarithmic spiral along with the discretization step ( $\Delta\theta$ ),  $30^\circ$  in our case. (B) Block diagram of the bioinspired grasping strategy. (C) Illustration of a biologically inspired grasping and manipulation strategy that can be implemented by controlling the cable forces (plotted in (D)). Starting from a state where the robot is packed into a spiral shape (Packing), increase the force applied to the right cable ( $F_2$ ) while keeping the left ( $F_1$ ) unchanged. The robot starts to uncurl from the root, reaching out towards the object (Reaching). After in contact with the object, by slowly reducing the force of the left cable while keeping the right unchanged the robot uncurls across the surface of the object (Climbing) to wrap around it. After this, the force of the right cable is increased to achieve a firm grasp (Grasping). (D) Illustration of the corresponding actuation pattern for the two cables used to produce the grasping and manipulation motion in (C). (E) An overview of the robot system and an image sequence for the real robot.

In order to implement the grasping strategy, we propose a state-aware approach based on motor current detection for automatically switching between the different behaviors (Fig. 4B). Starting from the *Packing* state, the robot unfolds and reaches out as the right cable is pulled at a constant speed (Stage 1: Reaching) (Fig. 5). When there is no contact with the object, the current of the right motor remains rather stable. If there is contact with an object, the robot is subjected to an external force so that the motor current increases to maintain a constant speed of motion. By detecting such an increase in current, the robot can perceive contact with an object. The threshold for contact detection is set through multiple experiments, where the maximum value of the current is recorded as the robot is running without contact. This simple mechanism is very effective and capable of detecting even the slightest contact (Fig. 5A and movie S3). After detecting the contact, the motor on the left switches from speed mode to torque mode and gradually decreases the torque down to

zero (Stage 2: Wrapping). That is, it slowly relaxes the left cable, letting the robot uncurl and climb along the surface of the object. When the torque of the left motor is zero, the wrap is completed. Then, the motor on the right pulls the cable at a constant speed to grasp the object to the root of the robot (Stage 3: Grasping). This method does not require external sensors, e.g., cameras or force sensors, and can realize high-precision contact sensing when grasping objects of different shapes (Fig. 5B and movie S4).

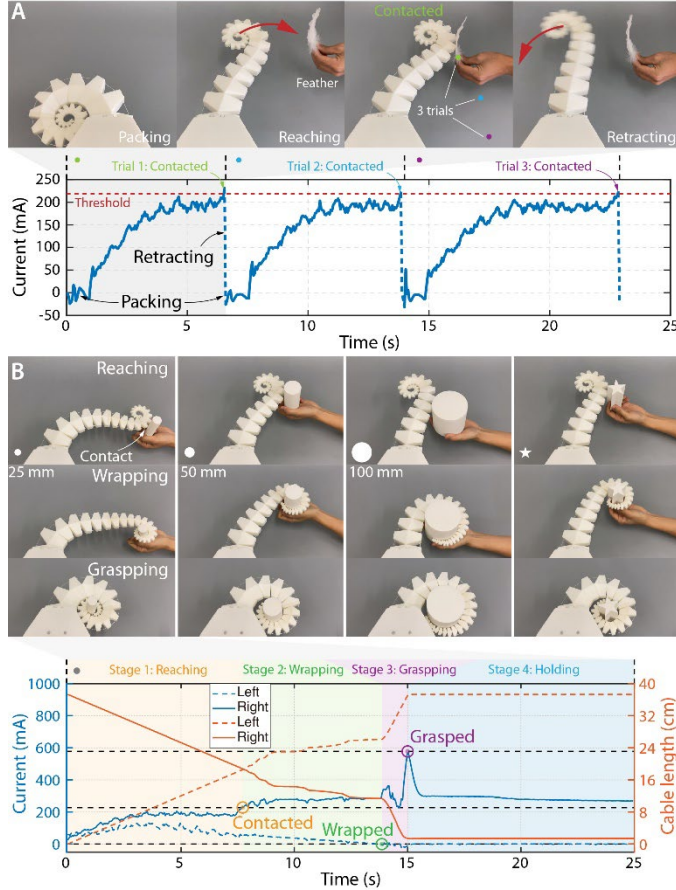


**Fig. 5. Contact detection and automatic grasping based on onboard current sensing. (A)**

By detecting changes in the current, the robot can sense contact with a feather. We placed a feather in three different positions and the robot retracted to the packing state as soon as it detected contact. The result shows that the same threshold can be used for contact detection across the workspace while keeping high sensitivity. The current signal of the right motor is plotted below the screenshots.

**(B)** The robot automatically grasps objects of different geometries. Stage 1: Reaching. The cables are pulled at a constant speed to make the robot reaching out. Contact is detected by monitoring the current value of the right motor. Stage 2: Wrapping. The left motor changes to the torque control mode, and the current is gradually reduced to zero and the wrapping of the object is completed. Stage 3: Grasping. The motor on the right moves at a constant speed until the current increases beyond a set value, whence the object is grasped to the root of the robot. Stage 4: holding. The robot holds the object by keeping cables at a constant length. The current signal of the motors and the length of the cables are plotted below the screenshots. The three black dashed lines from top to bottom are 0, contact detection threshold and grasping detection threshold.

## Manipulating various objects

To demonstrate the ability to grasp and manipulate a variety of objects, we first designed and fabricated a 2-cable SpiRob (45 cm in length) by 3D printing using soft filaments (Fig. S2A; another origami-based fabrication method is described in detail with Text S1). This robot was used to demonstrate the potential of the proposed spiral-shaped design principle and operating strategy. We tested for numerous objects varying in size, weight, and material. Unlike existing multimodal grasping mechanisms (31, 36, 37), the same spiral robot with the same strategy can successfully grasp and manipulate a wide variety of objects in size and weight (Fig. 6A-D, movie S5). Even in a confined space, the packed body can navigate through obstacles without relative sliding (Fig. 6 E, F, S6, and movie S6). Interestingly, we observed that the robot takes advantage of its interaction with the obstacles to reach the target instead of trying to avoid it. Since visual perception and control were not the focus in these experiments, we manually controlled the two cables like a puppet (implementation of a remote-control scheme with a joystick is detailed in Fig. S2, movie S7, and text S3). Evidently, given that the base of the robot is fixed in our experiments, objects need to be positioned in a suitable range.

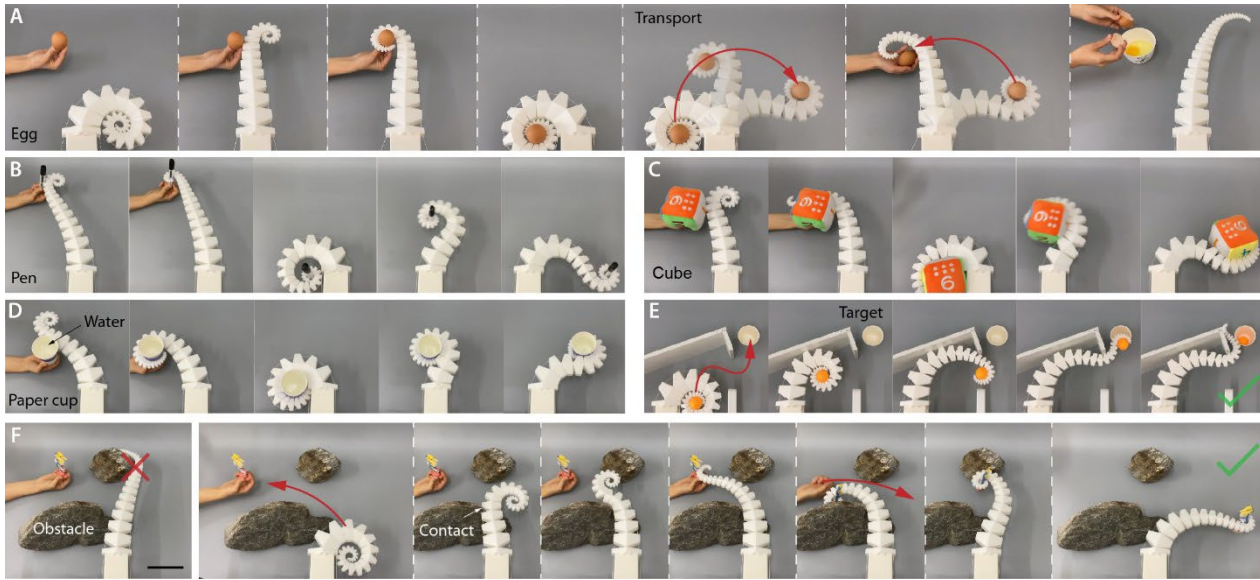


**Fig. 6. SpiRobs grasping and manipulating various objects.** (A)-(D) Image sequences of a two-cable spiral robot grasping and transporting a raw egg, a pen, a soft cube, and a paper cup filled with water, respectively. (E) The robot navigates through a door to transport a pingpong ball to its target in an S-shape trajectory. (F) Manipulation in confined space: the robot actively interacts with obstacles before reaching to grasp. These experiments demonstrate that the spiral robot can perform complex manipulation tasks by capitalizing on interactions with the environment. Scale bar in (F) represents 10 cm.

### 3-cable SpiRobs

To further explore the capabilities of the spiral robots, we designed and fabricated a robot actuated by 3 cables evenly spaced on the circle corresponding to the cross section (Fig. 7A). The length of the robot is 75 cm (tip/root diameter is 5 mm/72 mm), demonstrating that the spiral design principle can be easily extended to different scales. The choice of the cross section serves to reduce inertia and also increase the contact surface when grasping. Using a strategy similar to the 2D grasping, the 3D robot unfolds the curled body on the surface of the object to wrap and grasp it (Fig. 7B and movie S12). By controlling the cables complex paths can be achieved (Fig. 7C). Even very thin objects can be gripped with high stability for a non-slip grip (Fig. 7D, E and, movie S13).

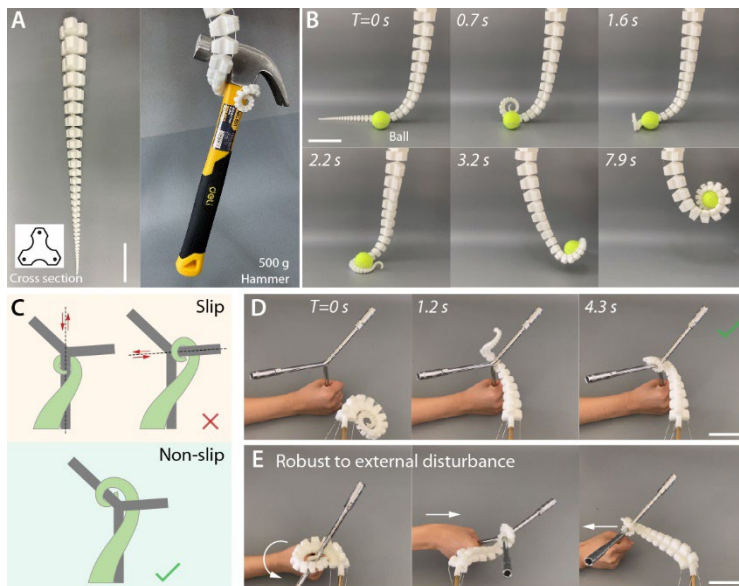


**Fig. 7. 3-cable SpiRobs.** (A) Photographs of a 75 cm long 3-cable spiral robot and its wrapping around a 500 g hammer. (B) Image sequence of a 3-cable SpiRob grasping a ball. (C) Illustration of a non-slip grasping strategy for the case of a tree-fork-shaped object. (D) Image sequence of a 3-cable spiral robot implementing the strategy to lift a hexagonal wrench. (E) Images showing the robustness of the strategy under external forces. The scale bars in (A) and (B) represent 10 cm and in (D) and (E) represent 5 cm.



## SpiRobs conducting dynamic tasks

We further illustrate that the presented class of soft robots portrays similar capabilities as in living organisms: high-speed dynamic movement and impact resistance with robust grasping. On sub-second or second timescale, octopuses can grab and catch a fish, while elephants can use their trunks to spray water all over their bodies. For most existing soft manipulators, achieving dynamic efficiency comparable to biological structures is merely impossible, despite having soft bodies. We observed that the open-loop behavior (movie S8) of SpiRob enables grasping within 60 ms (Fig. 8A, movie S1) and throwing at a speed of 8 m/s (Fig. 8B, S7, and movie S9). Its ability to passively deform allows grasping objects moving at high speeds (Fig. 8C, movie S10). Last but not least, the robot shows excellent grasping stability that can resist out-of-plane torsion and dynamic impact (Fig. 8D, movie S11). For dynamic operation in the 3D space, the shapes and moving patterns that the cable actuation can generate are more complicated due to the intrinsic inertia and stiffness of the body as well as the effect of gravity (movie S12). The curled body "shoots" out to reach a specific position (Figs. 8E, S8, Text S6, and movie S14) or grasp objects (Fig. 8F and movie S15).

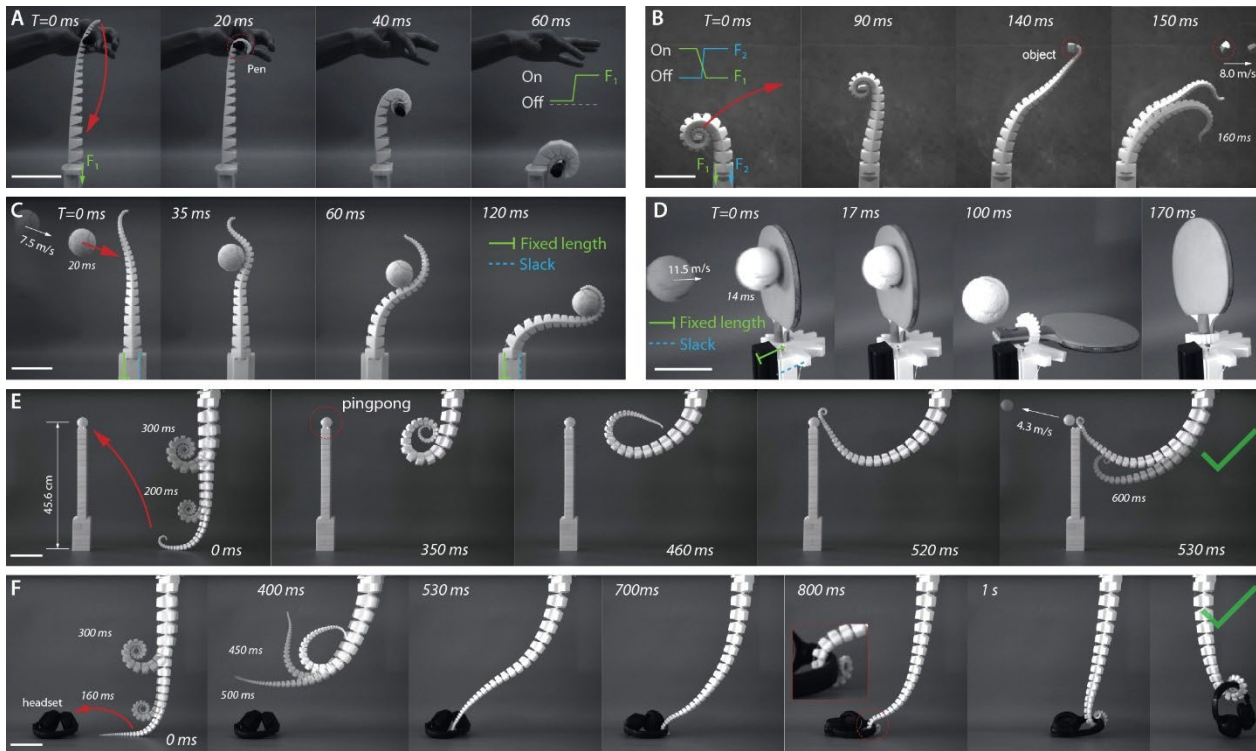


**Fig. 8. Dynamic tasks.** (A) Image sequence of dynamic grasping. The experiment shows that the robot finishes a fast-grasping within 0.06 s. The actuation pattern is displayed in the upper right corner where 'On' means that the cable is stretched and 'Off' means that the cable is slack. (B) Elephant throw. A robot 35 cm in length throws a piece of rubber at a speed of 8 m/s. (C) Passive grasping. Exploiting its passive compliance, the robot is capable of grasping a high-speed moving object within 100 ms even without control (the left cable is fixed to maintain a constant length while the right cable is slack). (D) Robust grasping. The robot holds the racket steadily as a 60 g tennis hits at 11.5 m/s (producing an average out-of-plane impact force of 138 N). (E) Whipping. The robot dynamically reaches a point in the 3D space on a sub-second timescale to pounce a pingpong ball. (F) The robot grasps and lifts a headset within 1 s. Scale bars in (A)-(F) represent 10 cm.



## DISCUSSION

This paper proposed a modular and interpretable principle for designing soft robots across different scales and presented a series of spiral robots that can grasp and manipulate objects through wrapping. By tensioning the cables, the robot reproduces a spiral-shaped wrapping behavior that is common in nature. A bioinspired strategy allows controlling the curling direction so as to handle objects that vary in size by more than two orders of magnitude and up to 260 times self-weight. Our results corroborate that the spiral-shaped principle constitutes an effective solution for the structural design of soft-engineered systems to exploit wrapping as a paradigm for versatile grasping and manipulation.

The design principle of the logarithmic spiral is a key novelty in this paper. Different from most soft robotic systems (13) where the hardware is designed first and the models are developed afterwards, in our system modeling (logarithmic spiral) comes first, and design/fabrication is a direct outcome of the model. This allows designing SpiRobs to meet the requirements of a large diversity of application scenarios (i.e., in terms of grasping size and load capacity, see Table S1), instead of using a trial (physically building the robot) and error (testing) approach. In addition, unlike the Piecewise Constant Curvature (PCC) model commonly used in the field (38, 39) (Fig. S9 A and B), the logarithmic spiral features faster curvature changes along the body (Fig. S9 C), thus resulting in a higher degree of flexibility. Most existing soft manipulators gain increased flexibility through the combination of multiple independently actuated segments (40–42). However, increasing the number of segments also increases the complexity of modeling and control (43). We show that based on a simple control strategy, SpiRob can achieve complex operations by controlling only two/three cables.

The presented SpiRobs feature regular discrete units, which is a distinctive feature that distinguishes them from other existing soft manipulators (19, 29, 30, 40, 44). The discretization introduces a series of internal constraints, which physically constrained the maximum curvature of each part of the robot body (that is, the curvature reaches the maximum when adjacent units touch each other). We found that the internal constraints not only improve the stability of grasping but also allow the robots to achieve wrapping with simple control laws. These constraints are key to realizing the logarithmic spiral-shaped wrapping. In nature, this internal constraint is reflected in the limited rotation angle between the adjacent bones of the skeletal organs (e.g., the tail of chameleons and seahorses) and the limited distance of muscle contraction in the muscular hydrostatic structure (e.g., the tentacles of octopuses and the trunks of elephants). However, for most existing soft octopus-tentacle or elephant-trunk inspired designs (Fig. S9A), whether driven by tensile actuators or fluids, deformations of the robot always increase with increasing actuation in the absence of structural curvature regulations. A similar design was presented in (45), where the cable-driven robot also features discrete units. However, the length of each unit is the same making the robot deform in a PCC manner. We emphasize that all geometric parameters of SpiRobs can be fully determined by the equation of the logarithmic spiral (e.g., the length and shape of units, the size of gaps, see Table S1).

The bioinspired grasping strategy shows large adaptability and high grasping stability. To climb on the surface of an object, the SpiRob makes full use of its interaction with it. However, these interactions exert forces on the object. If the object is not fixed, it will be moved when the robot touch it. This strategy has a higher success rate in grasping objects that are handed over by humans. The 3-cable SpiRob shows its ability to grasp a ball placed on the table without bumping it away. Moreover, our current work does not yet involve the visual perception of the robot and its environment, thus the motion in some experiments is controlled through direct manipulation of cables like a puppet (Figs. 6, 7, and 8).

## MATERIALS AND METHODS

### Conceptual design of a soft spiral robot

SpiRob consists of three main components: the robot body, the cables, and the motors. The two ends of each cable are connected to the tipmost unit and the motor, and the cable's contract/relax actuation is translated to the curling/uncurling motion of the robot, respectively. In the following, we describe the design process and determine the key parameters of the robot body.

We take a spiral robot with two cables that can wrap in two directions on a plane as an example. Recall the expression of a logarithmic spiral ( $(\rho, \theta)$  are polar coordinates):

$$\rho(\theta) = ae^{b\theta}, \quad b = \cot \psi, \quad (1)$$

where  $a$  is a scaling factor and  $b$  is the cotangent of the constant polar tangential angle  $\psi$  - defined as the angle between the tangent of a point on the spiral and the line connecting the point to the origin (Fig. S1A). Equation (1) can be re-written as  $\rho = e^{b(\theta + \frac{\ln a}{b})}$ , so that  $a$  can be interpreted as translation in the angle domain and  $b$  as scaling. For design, we restrict attention to the range  $\theta \geq 0$ . The regime  $\theta < 0$  corresponds to the extension from the tip to the point where the outer edges of the robot meet ( $\theta \rightarrow -\infty$ ). We define the 'central' spiral characterizing the central axis of the robot (Fig. S1B) by:

$$\rho_c(\theta) = \frac{1}{2}(ae^{b(\theta+2\pi)} + ae^{b\theta}) = \frac{a}{2}(e^{2\pi b} + 1)e^{b\theta}. \quad (2)$$

The rays starting from the origin and at fixed angle intervals ( $\Delta\theta = 30^\circ$  in our case) intersect with points on the original spiral and the central spiral which are connected to form quadrilateral areas (Fig. S1C and D). This forms one part of the robot, to which we attach an elastic layer that provides the restoring force that allows the robot to reach different directions (Fig. S1F). The other part is obtained by mirroring with respect to the central axis (and thus its contour follows an 'outer' spiral). In our design, the elastic layer's thickness is 5% – 10% of the unit width (5% for the 2-cable and 10% for the 3-cable robot in our implementation, see also Fig. S1F).

The taper angle ( $\phi$ ) of the robot has the following relationship with the spiral parameters:

$$\phi = 2 \arctan \left( \frac{\frac{1}{2}\delta(\theta)}{\int_{-\infty}^{\theta} \rho_c(\theta) d\theta} \right) = 2 \arctan \left( \frac{b(e^{2\pi b} - 1)}{e^{2\pi b} + 1} \right), \quad (3)$$

$$\delta(\theta) = ae^{b(\theta+2\pi)} - ae^{b\theta}, \quad (4)$$

where  $\delta(\theta)$  is the width of the robot at angle  $\theta$ . The integral in the denominator in equation (3) captures the length of the central spiral starting  $\theta = -\infty$  (see Fig. S1E). The taper angle  $\phi$  is independent of  $\theta$ , see equation (3), indicating that the spiral is tapered when expanded (Fig. S1E). The length ( $L_r$ ) of the (central axis of the) robot has the following relationship with the spiral parameters:

$$L_r = \int_0^{\theta_0} \rho_c(\theta) d\theta = \frac{a(e^{2\pi b} + 1)(e^{b\theta_0} - 1)}{2b}. \quad (5)$$

The lower bound of the integral here is  $\theta = 0$ , which corresponds to the tip of the robot (Fig. S1E). The curvature of the robot  $\kappa(\theta)$  (when packed into a logarithmic spiral) can be calculated from the expression of the central spiral to be:

$$\kappa(\theta) = \frac{2}{a(e^{2\pi b} + 1)\sqrt{b^2 + 1}} e^{-b\theta}. \quad (6)$$

In particular, the curvature changes exponentially fast with  $\theta$ . This renders inappropriate for our case the Piecewise Constant Curvature (PCC) model (38) that is commonly used for modeling and control of soft robots. Moreover, the deformation rate ( $\gamma$ ) of the robot's surface when it shifts from the packed state pointing to the left to the packed state pointing to the right (or vice versa) can be calculated as:

$$\gamma = \frac{\int_{\theta_0}^{\theta_0+2\pi} \rho(\theta) d\theta}{\int_0^{\theta_0} \rho(\theta) d\theta} = e^{2\pi b}, \quad (7)$$

For example, when  $b = 0.2199$  (i.e., taper angle  $\phi = 15^\circ$  in this case),  $\gamma = 3.98$ , which indicates the challenges to design and fabricate spiral robots with a continuous homogeneous body to undergo such large deformation. This is because repeated stretching/shortening at such a deformation rate can cause the material used to construct the robot (for instance, Silica gel) to break. We believe that this phenomenon also provides a justification for the wrinkles and folds observed on the surface of the elephant trunk that serve to provide additional flexibility for large deformations (46).

The design of a 3-cable robot that can curl in the 3D space follows the same concept as building a 2-cable robot (Fig. S1G). The difference is that the mirroring is in 3D (i.e., it gives a cone). Each three-dimensional unit is a fragment of the cone, so that without any alteration this would give a small contact surface when grasping an object. For this reason, we reshaped the cross section to increase the contact area (Fig. S1G). A similar feature of "square" cross section that improves mechanical performance in grasping has been observed in seahorse tails (4).

### Fabrication of SpiRob

The robot bodies are built using an existing 3D printing method. Specifically, we use a desktop 3D printer (X1 Carbon, Bambu Lab) together with 1.75mm TPU (Thermoplastic polyurethanes) filament (eTPU-95A, Esun) to fabricate our robots (Fig. S2A). We designed small holes on each unit for the cable to pass through (we provide a printable .stl file in the supplementary material). We use UHMWPE (ultra-high molecular weight polyethylene) cables for the actuation of the robot. This type of cable is wear-resistant and smooth, thus reducing friction as it moves through the robot's body. Furthermore, the cable is fastened to the tip unit with a fisherman knot to ensure that the actuation force is transmitted without slipping. We have made several observations that are pivotal in achieving modularity of the fabrication process. First, note that the scales of adjacent units of the robot are in a fixed ratio  $\beta$ , given by:

$$\beta = \frac{\delta(\theta+\Delta\theta)}{\delta(\theta)} = e^{b\Delta\theta}, \quad (8)$$

where  $\delta(\theta)$  is the width as at angle  $\theta$  defined in equation (4) and  $\Delta\theta$  is the discretization step. Thus, we only need to design one unit, and then scale up/down according to the factor  $\beta$  to obtain the design of all other units. Second, longer robots can be fabricated in segments that are then connected by a dovetail tenon connector (Fig. S2A). The 2-cable robot used in Figs. 4-6 consists of two segments, and the 3-cable robot in Fig. 7 consists of three segments.

### Control terminal

We built a motor control terminal (Fig. 4E), which consists of two motors (GM6020, DJI), an embedded controller (Robomaster Development Board, type A, DJI), and a 24V battery. The motors are direct-drive brushless without gearbox and can be controlled in terms of torque, speed, and position. This provides the basis for our current-based contact detection and wrapping-based grasping.

### Data analysis

The motor current, speed, and position data are captured using STM32Cube Monitor (data files S1 and S2). The length of the cable (Fig. 5B) is converted from the recorded rotor position of the motors in MATLAB. For dynamic tasks (Fig. 8), videos and screenshots are captured using a high-speed camera (ACS-3, NAC Image Technology).



## References and Notes

1. J. K. A. Langowski, P. Sharma, A. L. Shoushtari, In the soft grip of nature. *Sci. Robot.* **5**, eabd9120 (2020).
2. R. Hodson, A gripping problem. *Nature.* **557**, S23–S25 (2018).
3. G.-Z. Yang, J. Bellingham, P. E. Dupont, P. Fischer, L. Floridi, R. Full, N. Jacobstein, V. Kumar, M. McNutt, R. Merrifield, B. J. Nelson, B. Scassellati, M. Taddeo, R. Taylor, M. Veloso, Z. L. Wang, R. Wood, The grand challenges of *Science Robotics*. *Sci. Robot.* **3**, eaar7650 (2018).
4. M. M. Porter, D. Adriaens, R. L. Hatton, M. A. Meyers, J. McKittrick, Why the seahorse tail is square. *Science.* **349**, aaa6683 (2015).
5. M. Cianchetti, A. Arienti, M. Follador, B. Mazzolai, P. Dario, C. Laschi, Design concept and validation of a robotic arm inspired by the octopus. *Mater. Sci. Eng. C.* **31**, 1230–1239 (2011).
6. M. W. Hannan, I. D. Walker, Analysis and experiments with an elephant's trunk robot. *Adv. Robot.* **15**, 847–858 (2001).
7. *Springer handbook of robotics* (Springer Berlin Heidelberg, New York, NY, 2nd edition., 2016).
8. M. DeDonato, V. Dimitrov, R. Du, R. Giovacchini, K. Knoedler, X. Long, F. Polido, M. A. Gennert, T. Padır, S. Feng, H. Moriguchi, E. Whitman, X. Xinjilefu, C. G. Atkeson, Human-in-the-loop Control of a Humanoid Robot for Disaster Response: A Report from the DARPA Robotics Challenge Trials. *J. Field Robot.* **32**, 275–292 (2015).
9. L. Zhang, J. Zhao, P. Long, L. Wang, L. Qian, F. Lu, X. Song, D. Manocha, An autonomous excavator system for material loading tasks. *Sci. Robot.* **6**, eabc3164 (2021).
10. F. Xu, B. Wang, J. Shen, J. Hu, G. Jiang, Design and Realization of the Claw Gripper System of a Climbing Robot. *J. Intell. Robot. Syst.* **89**, 301–317 (2018).
11. J. Mahler, M. Matl, V. Satish, M. Danielczuk, B. DeRose, S. McKinley, K. Goldberg, Learning ambidextrous robot grasping policies. *Sci. Robot.* **4**, eaau4984 (2019).
12. K. Tai, A.-R. El-Sayed, M. Shahriari, M. Biglarbegian, S. Mahmud, State of the Art Robotic Grippers and Applications. *Robotics.* **5**, 11 (2016).
13. D. Rus, M. T. Tolley, Design, fabrication and control of soft robots. *Nature.* **521**, 467–475 (2015).
14. C. Majidi, Soft Robotics: A Perspective—Current Trends and Prospects for the Future. *Soft Robot.* **1**, 5–11 (2014).
15. R. F. Shepherd, F. Ilievski, W. Choi, S. A. Morin, A. A. Stokes, A. D. Mazzeo, X. Chen, M. Wang, G. M. Whitesides, Multigait soft robot. *Proc. Natl. Acad. Sci.* **108**, 20400–20403 (2011).
16. M. Wehner, R. L. Truby, D. J. Fitzgerald, B. Mosadegh, G. M. Whitesides, J. A. Lewis, R. J. Wood, An integrated design and fabrication strategy for entirely soft, autonomous robots. *Nature.* **536**, 451–455 (2016).
17. C. Laschi, B. Mazzolai, M. Cianchetti, Soft robotics: Technologies and systems pushing the boundaries of robot abilities. *Sci. Robot.* **1**, eaah3690 (2016).
18. A. Pal, D. Goswami, R. V. Martinez, Elastic Energy Storage Enables Rapid and Programmable Actuation in Soft Machines. *Adv. Funct. Mater.* **30**, 1906603 (2020).
19. A. D. Marchese, D. Rus, Design, kinematics, and control of a soft spatial fluidic elastomer manipulator. *Int. J. Robot. Res.* **35**, 840–869 (2016).
20. H. Jiang, Z. Wang, Y. Jin, X. Chen, P. Li, Y. Gan, S. Lin, X. Chen, Hierarchical control of soft manipulators towards unstructured interactions. *Int. J. Robot. Res.* **40**, 411–434 (2021).
21. E. Brown, N. Rodenberg, J. Amend, A. Mozeika, E. Steltz, M. R. Zakin, H. Lipson, H. M. Jaeger, Universal

- robotic gripper based on the jamming of granular material. *Proc. Natl. Acad. Sci.* **107**, 18809–18814 (2010).
22. F. Ilievski, A. D. Mazzeo, R. F. Shepherd, X. Chen, G. M. Whitesides, Soft Robotics for Chemists. *Angew. Chem. Int. Ed.* **50**, 1890–1895 (2011).
  23. S. Li, J. J. Stampfli, H. J. Xu, E. Malkin, E. V. Diaz, D. Rus, R. J. Wood, "A Vacuum-driven Origami "Magic-ball" Soft Gripper" in *2019 International Conference on Robotics and Automation (ICRA)* (IEEE, Montreal, QC, Canada, 2019; <https://ieeexplore.ieee.org/document/8794068/>), pp. 7401–7408.
  24. T. J. Jones, E. Jambon-Puillet, J. Marthelot, P.-T. Brun, Bubble casting soft robotics. *Nature*. **599**, 229–233 (2021).
  25. R. V. Martinez, J. L. Branch, C. R. Fish, L. Jin, R. F. Shepherd, R. M. D. Nunes, Z. Suo, G. M. Whitesides, Robotic Tentacles with Three-Dimensional Mobility Based on Flexible Elastomers. *Adv. Mater.* **25**, 205–212 (2013).
  26. I. Must, E. Sinibaldi, B. Mazzolai, A variable-stiffness tendril-like soft robot based on reversible osmotic actuation. *Nat. Commun.* **10**, 344 (2019).
  27. C. Jiang, D. Wang, B. Zhao, Z. Liao, G. Gu, Modeling and inverse design of bio-inspired multi-segment pneu-net soft manipulators for 3D trajectory motion. *Appl. Phys. Rev.* **8**, 041416 (2021).
  28. N. Giri, I. Walker, Continuum robots and underactuated grasping. *Mech. Sci.* **2**, 51–58 (2011).
  29. C. Laschi, M. Cianchetti, B. Mazzolai, L. Margheri, M. Follador, P. Dario, Soft Robot Arm Inspired by the Octopus. *Adv. Robot.* **26**, 709–727 (2012).
  30. H. Jiang, X. Liu, X. Chen, Z. Wang, Y. Jin, X. Chen, "Design and simulation analysis of a soft manipulator based on honeycomb pneumatic networks" in *2016 IEEE International Conference on Robotics and Biomimetics (ROBIO)* (IEEE, Qingdao, China, 2016; <http://ieeexplore.ieee.org/document/7866347/>), pp. 350–356.
  31. Z. Xie, A. G. Domel, N. An, C. Green, Z. Gong, T. Wang, E. M. Knubben, J. C. Weaver, K. Bertoldi, L. Wen, Octopus Arm-Inspired Tapered Soft Actuators with Suckers for Improved Grasping. *Soft Robot.* **7**, 639–648 (2020).
  32. Z. Zhang, X. Wang, D. Meng, B. Liang, Bioinspired Spiral Soft Pneumatic Actuator and Its Characterization. *J. Bionic Eng.* **18**, 1101–1116 (2021).
  33. J. Zhang, Y. Hu, Y. Li, K. Ma, Y. Wei, J. Yang, Z. Wu, H. Rajabi, H. Peng, J. Wu, Versatile Like a Seahorse Tail: A Bio-Inspired Programmable Continuum Robot For Conformal Grasping. *Adv. Intell. Syst.*, 2200263 (2022).
  34. M. Calisti, M. Giorelli, G. Levy, B. Mazzolai, B. Hochner, C. Laschi, P. Dario, An octopus-bioinspired solution to movement and manipulation for soft robots. *Bioinspir. Biomim.* **6**, 036002 (2011).
  35. K. Salisbury, W. Townsend, B. Ebrman, D. DiPietro, "Preliminary design of a whole-arm manipulation system (WAMS)" in *1988 IEEE International Conference on Robotics and Automation Proceedings* (1988), pp. 254–260 vol.1.
  36. D. Morrison, A. W. Tow, M. McTaggart, R. Smith, N. Kelly-Boxall, S. Wade-McCue, J. Erskine, R. Grinover, A. Gurman, T. Hunn, D. Lee, A. Milan, T. Pham, G. Rallos, A. Razjigaev, T. Rowntree, K. Vijay, Z. Zhuang, C. Lehnert, I. Reid, P. Corke, J. Leitner, "Cartman: The Low-Cost Cartesian Manipulator that Won the Amazon Robotics Challenge" in *2018 IEEE International Conference on Robotics and Automation (ICRA)* (IEEE, Brisbane, QLD, 2018), pp. 7757–7764.
  37. B. Fang, F. Sun, L. Wu, F. Liu, X. Wang, H. Huang, W. Huang, H. Liu, L. Wen, Multimode Grasping Soft Gripper Achieved by Layer Jamming Structure and Tendon-Driven Mechanism. *Soft Robot.* **9**, 233–249 (2022).
  38. R. J. Webster, B. A. Jones, Design and Kinematic Modeling of Constant Curvature Continuum Robots: A Review. *Int. J. Robot. Res.* **29**, 1661–1683 (2010).
  39. I. D. Walker, Continuous Backbone "Continuum" Robot Manipulators. *ISRN Robot.* **2013**, 1–19 (2013).

40. M. D. Grissom, V. Chitrakaran, D. Dienno, M. Csencits, M. Pritts, B. Jones, W. McMahan, D. Dawson, C. Rahn, I. Walker, "Design and experimental testing of the OctArm soft robot manipulator" in, G. R. Gerhart, C. M. Shoemaker, D. W. Gage, Eds. (Orlando (Kissimmee), FL, 2006; <http://proceedings.spiedigitallibrary.org/proceeding.aspx?doi=10.1117/12.665321>), p. 62301F.
41. Z. Gong, X. Fang, X. Chen, J. Cheng, Z. Xie, J. Liu, B. Chen, H. Yang, S. Kong, Y. Hao, T. Wang, J. Yu, L. Wen, A soft manipulator for efficient delicate grasping in shallow water: Modeling, control, and real-world experiments. *Int. J. Robot. Res.*, 027836492091720 (2020).
42. T. George Thuruthel, E. Falotico, M. Manti, A. Pratesi, M. Cianchetti, C. Laschi, Learning Closed Loop Kinematic Controllers for Continuum Manipulators in Unstructured Environments. *Soft Robot.* **4**, 285–296 (2017).
43. T. George Thuruthel, Y. Ansari, E. Falotico, C. Laschi, Control Strategies for Soft Robotic Manipulators: A Survey. *Soft Robot.* **5**, 149–163 (2018).
44. A. Bajo, N. Simaan, Hybrid motion/force control of multi-backbone continuum robots. *Int. J. Robot. Res.* **35**, 422–434 (2016).
45. E. Coevoet, A. Escande, C. Duriez, Optimization-Based Inverse Model of Soft Robots With Contact Handling. *IEEE Robot. Autom. Lett.* **2**, 1413–1419 (2017).
46. A. K. Schulz, M. Boyle, C. Boyle, S. Sordilla, C. Rincon, S. Hooper, C. Aubuchon, J. S. Reidenberg, C. Higgins, D. L. Hu, Skin wrinkles and folds enable asymmetric stretch in the elephant trunk. *Proc. Natl. Acad. Sci.* **119**, e2122563119 (2022).